ACS APPLIED MATERIALS & INTERFACES

Research Article

www.acsami.org

Target Specific Delivery of Anticancer Drug in Silk Fibroin Based 3D Distribution Model of Bone−Breast Cancer Cells

Bano Subia, Tuli Dey, Shaily Sharma, and Subhas C Kundu*

Department of Biotechnology, Indian Institute of Technology Kharagpur, Kharagpur, West Bengal 721302, India

ABSTRACT: To avoid the indiscriminating action of anticancer drugs, the cancer cell specific targeting of drug molecule becomes a preferred choice for the treatment. The successful screening of the drug molecules in 2D culture system requires further validation. The failure of target specific drug in animal model raises the issue of creating a platform in between the in vitro (2D) and in vivo animal testing. The metastatic breast cancer cells migrate and settle at different sites such as bone tissue. This work evaluates the in vitro 3D model of the breast cancer and bone cells to understand the cellular interactions in the presence of a targeted anticancer drug delivery system. The silk fibroin based cytocompatible 3D scaffold is used as in vitro 3D distribution model. Human breast adenocarcinoma and osteoblast like cells are cocultured to evaluate the efficiency of doxorubicin loaded folic acid conjugated silk fibroin nanoparticle as drug delivery system. Decreasing population of the cancer cells, which lower the levels of vascular endothelial growth factors, glucose consumption, and lactate production are observed in the drug treated coculture constructs. The drug treated constructs do not show any major impact on bone mineralization. The diminished expression of osteogenic markers such as osteocalcein and alkaline phosphatase are recorded. The result indicates that this type of silk based 3D in vitro coculture model may be utilized as a bridge between the traditional 2D and animal model system to evaluate the new drug molecule (s) or to reassay the known drug molecules or to develop target specific drug in cancer research.

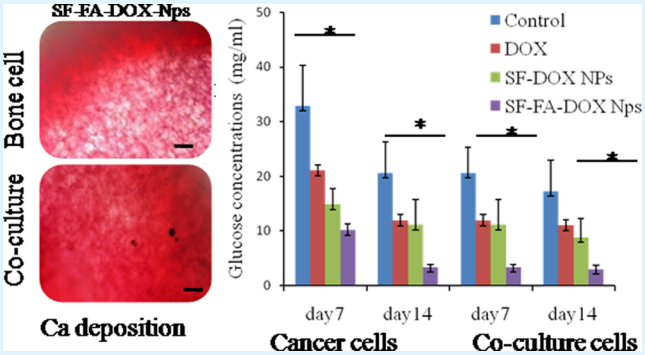

KEYWORDS: *silk fibroin, 3D in vitro model, coculture, drug delivery, bone metastasis*

1. INTRODUCTION

For cancer therapy, drug delivery systems are rapidly evolving to overcome the limitations of conventional chemotherapy. Traditional therapy shows many drawbacks such as nonspecific biodistribution and targeting, poor water solubility, and low therapeutic indices,[1] which need to be addressed. Nanosized drug delivery vehicles provide enhanced antitumor efficacy with reduced side effects, owing to their properties such as enhanced circulation time in blood, enhanced permeability retention effect, and active cellular uptake.[2,3] However, such successful applications seem to be underutilized due to their limited entry through oral and dermal route. The cancerous tissue is identified by highly expressed membrane receptors.[2] Of these, the folate receptor receives a great attention due to the enormous consumption of folate by the cancerous cells. The folate receptor is overexpressed on the vast majority of the cancerous cells/tissues, while its limited expression is recorded in healthy tissue and organs.[4] This supports its role as a candidate for target specific treatment. It is being selected for targeted delivery of the drug loaded nanoparticles. This is partially due to the ease of folic acid conjugation chemistry and availability of increased folate receptors in invasive tumors.[5] The goal of the folate-conjugated nanoparticle mediated drug delivery system is to deliver the drug at the target site while minimizing the accumulation at nontargeted site(s). The targeted particles enter the intercellular transport and thus avoid the immune system and increase the circulation time.[6] The most common approach used for escaping the reticuloendothilial system is to design the nanoparticles with neutral surface charge by coating them with polyethylene glycols and polysorbate to provide the hydrophilic environment. This helps to shield it from the immune recognition and to avoid the reticuloendothilial system. This leads to the long circulation time and provide stability for the nanoparticle complex in blood.[7] The recent research indicates that the folic acid conjugated with chitosan, bovine serum albumin, silk fibroin, and tumor microenvironment-sensitive polypeptides targets the cancer cells more effectively in 2D environment.[8−11] However, the folate conjugated nanovehicles in in vivo conditions could not meet the criteria for successful drug delivery system. The overexpression of folate receptors does little with the targeted drug delivery under in vivo condition.[12] It is reported that the albumin and PLGA conjugated with folate nanoparticles (targeted) do not show any significant differences from nontargeted nanoparticles in rodent tumor model.[13,14] Paulos et al. report that this may be due to the accumulation of folate in the liver and spleen of 5- to 6-week-old BALB/c and DBA-2 mice, which are the major

Received: September 12, 2014
Accepted: January 5, 2015
Published: January 5, 2015

DOI: 10.1021/am506094c
ACS Appl. Mater. Interfaces 2015, 7, 2269−2279

Table 1. Previously Reported Work Carried out on in Vitro 3D Tumor Model Using Different Systems[a]

system	materials	types of cells	anticancerous drug	refs
in vitro 3-D tumor model	silk fibroin scaffolds	breast cancer cells	no drug applied	27
	collagen gels embedded spheroids	epithelial, endothelial, fat and smooth muscle cells	no drug applied	32
	alginate hydrogel	epithelial carcinoma cell lines	paclitaxel	33
	PLG scaffolds	lung carcinoma, glioblastoma cell line, epithelial carcinoma cell lines	no drug used	34
coculture model	3D microscale perfusion-based two-chamber (3D-μPTC) tissue model	liver cells and glioblastoma multiform brain cancer cells	temozolomide and ifosfamide	35
	PEG hydrogles	human prostate cancer and bone cells	no drug applied	36
	2D system	human mesenchymal stem cells and prostate cancer cells	docetaxel	37
	poly(vinyl alcohol)- chitosan microparticles	breast cancer cells	doxorubicin paclitaxel and tamoxifen	38
	silk fibroin scaffolds	human breast adenocarcinoma, mesenchymal stem cells and osteoblast-like cells	no drug applied	39
drug screening in 3D model	poly(vinyl alcohol) -chitosan microparticles embedded 3D model	breast cancer cells	doxorubicin, paclitaxel and tamoxifen	38
	chitosan scaffolds	breast cancer cells	tamoxifen	40
	adipose tissue-derived extracellular matrix scaffolds	MCF-7, BT474, and SKBR3 cells	doxorubicin and lapatinib	41
	gelatin hydrogel scaffolds	breast cancer cells	doxorubicin	42
	silk fibroin scaffolds	breast cancer cells	paclitaxel, celecoxib, and ZD6474	43
nanoparticle mediated drug delivery in 3D scaffolds	silk fibroin-chitosan scaffolds	GILM2 breast cancer cells	embedded with liposomal nanoparticles loaded with emodin	44
	tumor spheroids	human ovarian carcinoma cell line	hyaluronan (HA) coated silica nanoparticles loaded with doxorubicin	45
	macroporous polycaprolactone scaffolds	human telomerase reverse transcriptase and human mesenchymal stem cells	embedded clay nanoparticles loaded with doxorubicin	46
	gold nanoparticles	human colon adenocarcinoma cell lines	no drug applied	47
	silk fibroin scaffolds (targeted drug delivery)	osteoblasts and cancer cells (coculture)	silk fibroin-folate conjugated nanoparticles loaded with doxorubicin	this study

[a]The table indicate latest scenario on the area of research intension of carrying out this work.

storage organs of excessive folate.[15] The accumulation of folate conjugated particles within the tumor depends upon the blood circulation, coating on the particles, and presence of the ligands on the nanoparticles surface.[15] The efficiency of receptor-mediated endocytosis depends on the concentration of the nanoparticles near the target cells, frequency of doses, particle size, ligands density, and surface charge.[16]

All these inconsistencies, between the in vitro (2D) and animal model study can be explained by the limitations of 2D conventional tissue culture system, which lacks the cell to cell and cell-extra cellular matrix interactions. Cancer research still typically depends on 2D in vitro study and animal model to investigate the tumor mechanism, angiogenesis, invasion, and metastasis[17] which lead to conflicting result due to the differences in cellular behavior, phenotypes, and gene expression.[18,19]

It is already felt that the in vitro 3D tumor model of interest needs to be designed for screening and testing of the drug effectively in order to bridge the gap between 2D system and in vivo condition. The 3D platforms in the form of hydrogel, scaffolds, and microfluidics can provide affective model for testing the drug delivery, dose dependent activity, metabolism, and toxicity due to their cell−cell, cell−matrix interactions, mass transport, and mechanical signals.[20] The reports are available where 3D constructs are used to understand the tumor organization and cellular interaction.[21] Several synthetic[22] and natural polymer[23,24] based scaffolds are used to simulate the tumor organization. The use of natural silk protein 3D fibroin based construct to model the breast tumor investigation established earlier.[25] 3D matrices of silk fibroin designed from *Antheraea mylitta* protein may be a good candidate for cancer research. The 3D fibroin scaffolds possess 84 kPa compressive strength,[26] whereas cell seeded fibroin scaffolds pose dynamic stiffness 42.5 kPa.[27] Higher compressive strength of fibroin scaffolds provides matrix stiffness, which regulate the cancer cell survival, metastatic dissemination, malignant transformation growth, and invasion.[28] The measured shear stiffness of the tumors ranges from 18 to 94 kPa and for adipose breast tissue in the breast cancer patients the shear stiffness ranges from 4 to 16 kPa.[29] This is close to the stiffness observed for *A. mylitta* (2%) scaffolds. The silk fibroin scaffolds facilitate the long-term cancer culture, and the cultured cancerous cells on the scaffolds show more aggressiveness than those cultured on other 3D culture systems.[30] The osteoblast like cells are also reported to successfully differentiate on *A. mylitta* silk scaffolds[31] making them a good candidate to investigate bone metastasis. The research being carried out on this area is presented to view at a glance in Table 1.

The present study is conceptualized to effectively bridge the gap between 2D system and in vivo condition, by fabricating the slowly degradable 3D fibroin scaffolds from non mulberry Indian tropical tasar silkworm *Antheraea mylitta* to model the 3D distribution of the bone−breast cancer cells. The efficiency of the folate conjugated fibroin nanoparticles loaded with anticancerous model drug doxorubicin is evaluated on the silk based 3D matrix system. A coculture construct is prepared with human osteoblast like cells and human breast adenocarcinoma cells to mimic the 3D microenvironment of bone−breast cancer

DOI: 10.1021/am506094c
ACS Appl. Mater. Interfaces 2015, 7, 2269−2279

Scheme 1. Schematic Illustration of Silk Fibroin Folate Conjugation

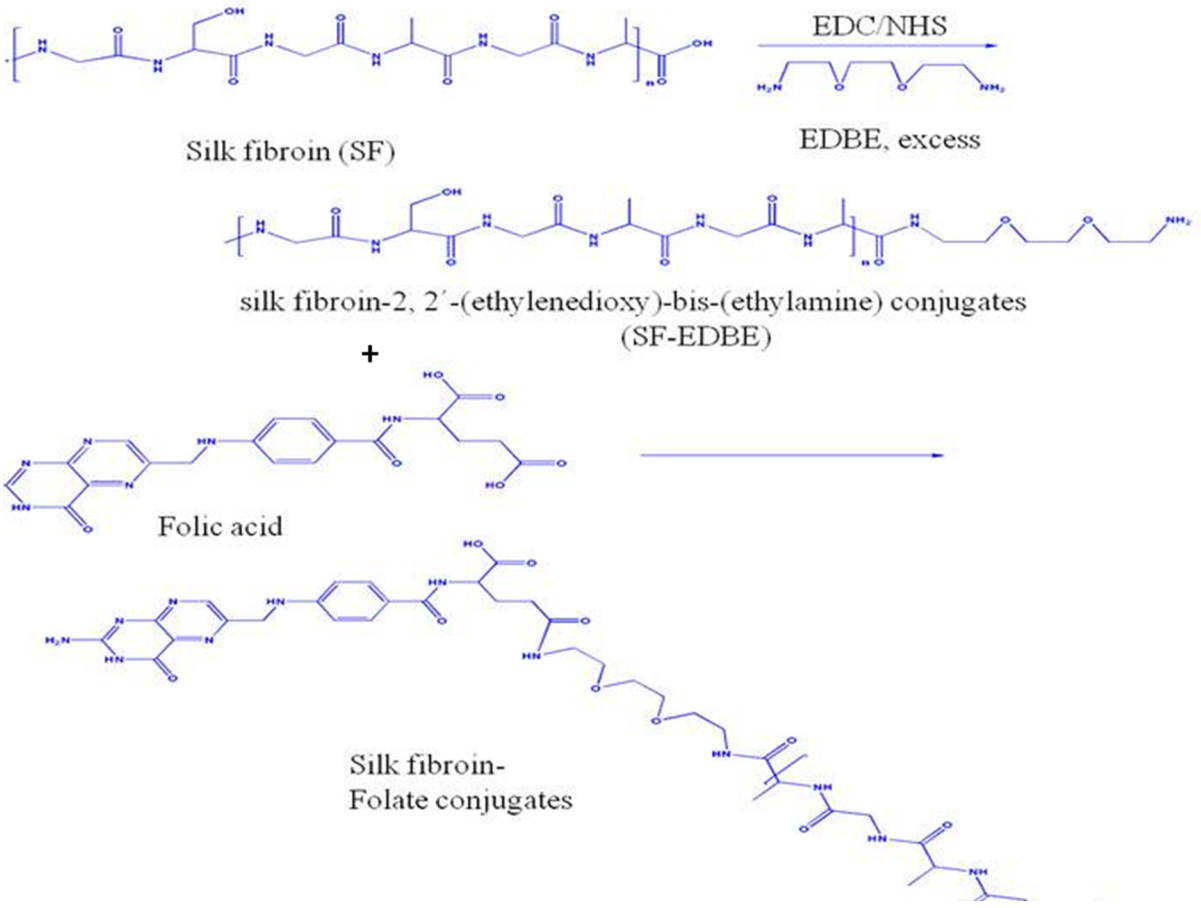

metastasis. The effect of the targeted drug delivery is investigated through the cell metabolic activity, bone mineralization, alkaline phosphatase, and osteogenic gene expressions. The invasive properties of the cancer cells such as glucose consumption, lactate production, and vascular endothelial growth factor release are also estimated.

2. MATERIALS AND METHODS

2.1. Materials. Mature live late fifth instar larvae of nonmulberry Indian tropical tasar silkworm *Antheraea mylitta* were collected from our (IIT Biotechnology) experimental farm. Folic acid, doxorubicin (Sigma-Aldrich, St Lewis USA), cellulose tubing of MWCO 12 kDa (Pierce, USA), acetone, glutaraldehyde, doxorubicin, DMSO (dimethyl sulfoxide), MTT (3-(4,5-dimethylthiazol-2-yl)-2,5-diphenyltetrazolium bromide), 2,2′-(ethylenedioxy) bis(ethylamine) (EDBE), *N*-hydroxy-succinimide (NHS) (Merck, India), and cell tracker red (CMTPX) and green (CMFDA) (Invitrogen, USA) were purchased for these experiments. Other chemicals used were of analytical grade.

2.2. Isolation and Regeneration of Silk Fibroin Protein from Silk Glands of *Antheraea mylitta*. The fully grown fifth instar larvae of *A. mylitta* (Am) silkworm were dissected for extraction of silk fibroin protein following a method described earlier. In brief, the posterior silk glands were isolated and washed in deionized water to remove traces of sericin. The glandular tubes are then squeezed with fine forceps to extrude out the protein. Isolated fibroin was dissolved using a mild anionic surfactant SDS (1%). The excess surfactant was removed by dialysis against water using dialysis membranes. The fibroin solution was collected, and the concentration was determined by gravimetric and colorimetric (Bradford) analysis.

2.3. Fabrication of Folate Conjugated Doxorubicin Loaded Silk Fibroin Nanoparticles. Folate conjugated fibroin nanoparticles were prepared by a method described earlier using carbodiimide chemistry and N hydroxyl coupling method.[10] The conjugation process is presented in Scheme 1.

2.4. Cell Culture. The osteoblasts like cells (MG63) and human adenocarcinoma (MDA-MB-231) cells were procured from National Centre for Cell Science (NCCS), Pune, India. The cells were maintained at 37 °C in a CO_2 incubator (with humidifier) in DMEM medium supplemented with 10% FBS and 1% penicillin/streptomycin solution. The cells were harvested by trypsin/EDTA solution at every third day.

2.5. Preparation of Coculture Constructs. 3D silk fibroin scaffolds of *A. mylitta* (Am) were carefully seeded into 24 well culture plates with (2:1) (1×10^5:0.5×10^5) ratio of osteoblast like cells (MG63) and human adenocarcinoma cells (MDA-MB-231). The constructs were supplemented with serum (10%) containing DMEM medium. The constructs were kept inside the incubator at 37 °C for 2 h to allow the cells to attach and settle into the scaffolds. After 2 h of incubation fresh medium were added. Media was replaced thrice in a week, and constructs were harvested after 7 and 14 days according to experimental setup. Constructs seeded with only human adenocarcinoma cells (MDA-MB-231) and osteoblast like cells (MG63) were used as control.

2.6. Analysis of Cellular Proliferation Assay on Monoculture and Coculture Constructs. Proliferation of osteoblast (MG63) (1:0), human adenocarcinoma cells (MDA-MB-231) (1:0) (monoculture), and coculture of osteoblast and cancer cells (2:1) on 3D silk fibroin matrices were evaluated by MTT assay. The total cell population was kept constant for all the population (1×10^5:0.5×10^5) cells/scaffolds. To evaluate the cytotoxicity of the drug loaded nanoparticles, cell seeded constructs were cultured for 7 and 14 days. Afterward, the scaffolds were serum starved for 24 h, and treated for 48 h with pure doxorubicin (20 μg/mL), silk fibroin (SF) nanoparticles (NPs) loaded with doxorubicin (SF-DOX NPs) (nontargeted) (20 μg/mL), and silk fibroin folate conjugated nanoparticles loaded with doxorubicin (SF-FA-DOX NPs) (targeted) (20 μg/mL). Treated and untreated (control) constructs were further used for MTT assay. The data accumulations were carried

DOI: 10.1021/am506094c
ACS Appl. Mater. Interfaces 2015, 7, 2269−2279

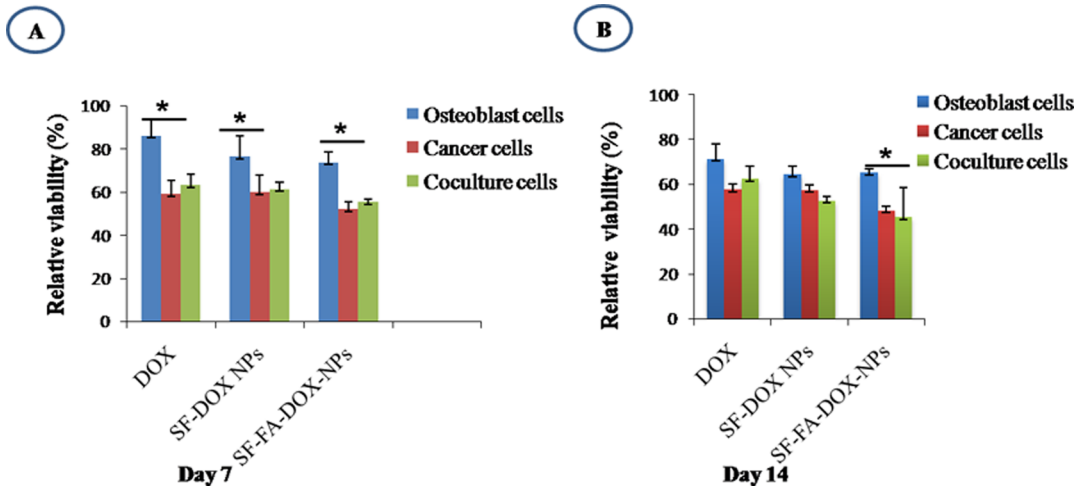

Figure 1. Cell proliferation assays of monoculture and coculture (osteoblast like cells and cancer cells) construct after treatment with doxorubicin, silk fibroin-doxorubicin, and silk fibroin-folate-doxorubicin loaded nanoparticles after 7 (A) and 14 days (B) of culture periods. Data are normalized with the control value (100%).

through the multiplate plate reader at 595 nm, and the absorbance values of three separate experiments (in triplicate) were plotted.

2.7. Cellular Morphology in Monoculture and Coculture Constructs. *a. Confocal Microscopy.* Attachment and spreading of osteoblast like cells (monoculture), cancer cells (monocultures), and coculture cells on fibroin 3D scaffolds were assessed after the treatment, using confocal microscopy. To analyze the cellular distribution, within the 3D scaffold, osteoblast and cancer cells were prestained with cell tracker green CMFDA (5-chloromethyl fluorescence diacetate; Invitrogen, 50 μg) and cell tracker red CMTPX (Invitrogen, 50 μg), respectively. The prestained osteoblast cells (1×10^5) and cancer cells (0.5×10^5) were seeded on *A. mylitta* scaffolds and cultured for 7 days. Afterward the cell seeded constructs were incubated with pure doxorubicin, doxorubicin loaded silk fibroin nanoparticles (nontargeted), and doxorubicin loaded silk fibroin folate nanoparticles (SF-FA-DOX) (targeted) for 48 h. The constructs were imaged by confocal laser scanning microscope (CLSM, Olympus FV 1000 attached with inverted microscope IX 81, Japan) equipped with Argon (488 nm) and He−Ne (534 nm) lasers. Two-dimensional multichannel sequential imaging and image processing was carried out by FV 1000 Advance software version 4.1 (Olympus, Japan).

b. Scanning Electron Microscopy. The cell seeded constructs were treated with pure DOX, SF-DOX NPs, and SF-FA-DOX NPs and incubated for 48 h. Treated scaffolds were fixed with 4% para-formaldehyde for 1 h and subjected to gradual dehydration followed by vacuum drying. Finally scaffolds were sputter-coated with gold and imaged by scanning electron microscope (JEOL-JSM 5800).

2.8. Osteogenesis in Drug Treated Scaffold. The cells were cultured for 14 days as mono (osteoblast) and coculture population on the 3D silk fibroin constructs and subjected to osteogenesis specific analysis after nanoparticle based drug delivery.

a. Alkaline Phosphatase Synthesis. The cell seeded constructs were cultured for 14 days and treated with DOX, SF-DOX- NPs, and SF-FA-DOX NPs for 48 h. The spent media was collected from the monoculture and coculture constructs and used for alkaline phosphatase (ALP) quantification by Kind and King's method (Cogent alkaline phosphatase diagnostic reagent kit, India). Briefly, the secreted alkaline phosphatase used to convert the phenyl phosphate of the reagent to inorganic phosphate and phenol at pH 10.0. The synthesized phenol reacts with the 4-aminoantipyrine and oxidizing agent (potassium ferricyanide) to form an orange-red colored complex, which can be measured colorimetrically. The color intensity is proportional to the enzyme activity. The ALP activity was determined by measuring the absorbance at 510 nm, and total protein content was determined by Bradford assay at 540 nm using microplate reader (Bio-Rad).

b. Calcium Deposition Assay. Calcium deposition was visualized using Alizarin Red S stain (Sigma-Aldrich, USA). Stain solution was prepared by dissolving Alizarin powder (1%) into water (pH was maintained between 4.1 and 4.3 using ammonium hydroxide solution). Scaffolds were fixed in paraformaldehyde (4%) for 15 min, cut into sections, rinsed in PBS and stained in Alizarin Red S solution for 2 min. Excess stain was removed by extensive washing, and then stained sections were mounted on slides and analyzed under Nikon inverted microscope (ECLIPSE TS100).

c. Analysis of Osteogenic Markers. Pure DOX, SF-DOX NPs, and SF-FA-DOX NPs treated mono (osteoblast) and coculture scaffolds were used for total RNA isolation using total RNA isolation kit (Qiagen) following the manufacturer's protocol. Isolated RNA was further treated with DNA removal kit procured from Life Technologies (Ambion DNA-free). Total RNA was subjected to cDNA synthesis using the first strand cDNA synthesis kit (Fermentas) and oligo(dT) primers. After that mRNA level of alkaline phosphatase (ALP) and osteocalcein (OC) were analyzed by semiquantitative RT-PCR reaction using custom-made forward and reverse primers (SI Table 2) in respect to GAPDH as internal control. PCR product was investigated through 1.5% agarose gel electrophoresis and densitometric analysis.

2.9. Analysis of Invasive Properties of Metastatic Breast Cancer Cell. The cells were cultured for 14 days as mono (adenocarcinoma) and coculture population on the 3D silk fibroin constructs and subjected to metastasis specific analysis after nanoparticle based drug delivery.

a. Angiogenesis. The amount of secreted VEGF present in culture medium of cancerous cells and coculture cells after treatment with pure DOX, SF-DOX NPs and SF-FA-DOX NPs was assessed by VEGF Elisa kit (R and D Technologies) by following the manufacture's protocol. VEGF level were assayed by using sandwich ELISA assay. Each assay condition was tested in triplicate. The data acquisitions were carried out at 450 nm using multiplate reader.

b. Glucose Consumption and Lactate Production Assay. The amount of glucose present in the culture media of samples after treatment with pure DOX, SF-DOX NPs, and SF-FA-DOX NPs was determined using the Glucose Assay Kit (GAGO-20 Sigma). Briefly, 2.5 μL of media was added to 100 μL of enzyme mixture and incubated at 37 °C for 30 min. The reaction was quenched with 100 μL of H_2SO_4 (12N) and the absorbance was measured using a microplate reader at 540 nm. Each measurement was performed in triplicate. The glucose concentration was calculated using triplicate of a single standard (0.05 mg/mL) according to manufacturer's protocol. The amount of glucose consumed was determined by subtraction of the total glucose present in the media with the glucose left on day 7 and 14 after seeding.

The lactate present in the media after drug treatment was assayed using Lactate assay kit (K607-100, Biovision) of cells grown for 7 and 14 day culture periods. The amount of lactate produced by the cells after drug treatment was measured at 570 nm.

2.10. Statistical Analysis. Three samples were used in each group, and the results were reported as means ± standard deviations. All the experiments were performed three times. Student *t* test was performed, and $p \leq 0.05$ was considered significant.

DOI: 10.1021/am506094c
ACS Appl. Mater. Interfaces 2015, 7, 2269−2279

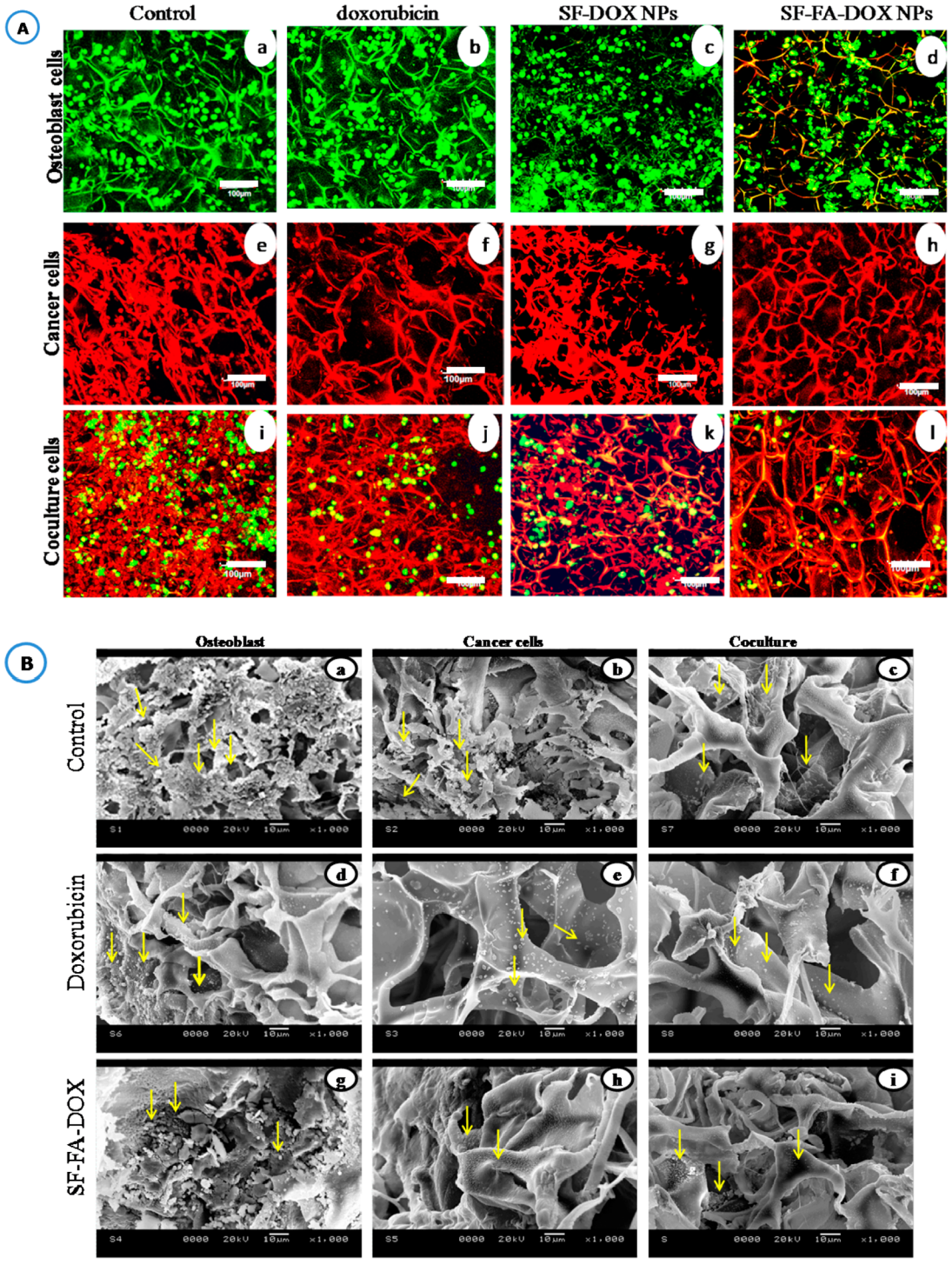

Figure 2. Analysis of cellular distribution and morphology in mono and coculture construct. (A) Confocal microscopy results show the growth and proliferation of monoculture cells (osteoblast like cells and cancer cells) and coculture cells after treatment with pure doxorubicin, nontargeted and targeted doxorubicin after 7 days of culture period. The osteoblast cells are stained with cell tracker green (a–d) and the cancerous cells (e–h) are treated with cell tracker red and coculture cells show mixed population green and red (i–l). Scale bar represents 100 μm. (B) SEM images of monoculture cells (osteoblast like cells and adenocarcinoma cells) and coculture cells (a–c), after treatment of doxorubicin (d–f), and targeted doxorubicin (g–i) after 7 days of culture time period. The yellow arrows indicate the cells.

3. RESULTS

3.1. Analysis of Cellular Proliferation, Distribution and Morphology within Drug Treated Monoculture and Coculture Constructs. *a. Cell Metabolic Activity.* In vitro cytotoxicity assays of pure doxorubicin, nontargeted doxorubicin, and targeted doxorubicin are carried out on monoculture (osteoblasts, cancerous cells) and coculture constructs. The assay suggests a significant change in the cell metabolic activity of the drug treated constructs due to the lowered reduction of tetrazolium blue dye. The results demonstrate that the cell viability and proliferation of monoculture cancerous cells and

DOI: 10.1021/am506094c
ACS Appl. Mater. Interfaces 2015, 7, 2269–2279

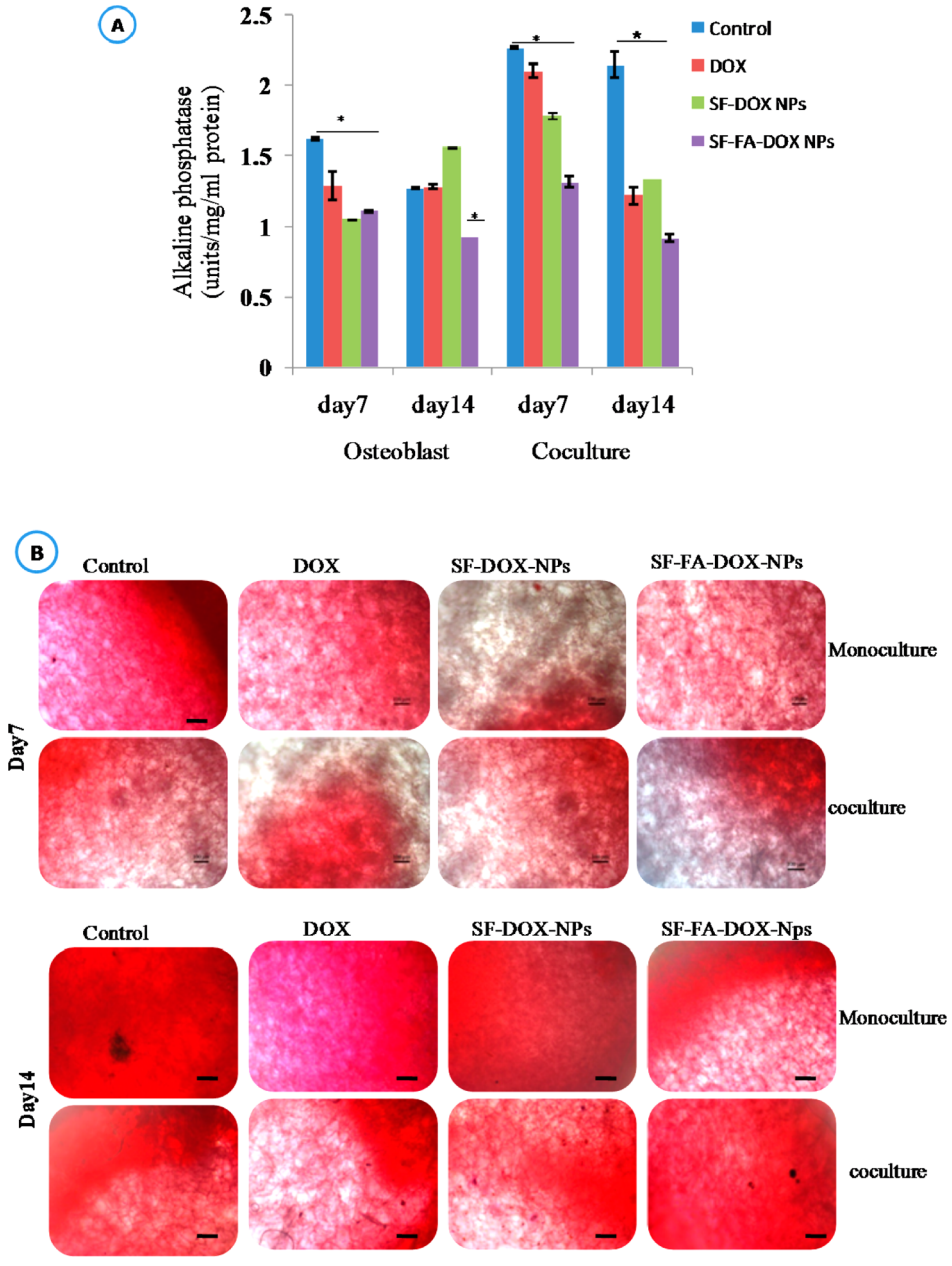

Figure 3. Functional analysis of osteogenesis in mono and coculture constructs. (A) Analysis of alkaline phosphatase acitivity in coculture and osteoblast like cells (control) after treatment with pure doxorubicin, nontargeted doxorubicin and targeted doxorubicin after 7 and 14 days culture periods. (B) Calcium deposition in coculture cells and osteoblast like cell seeded constructs (control) after treatment with pure doxorubicin (DOX), silk fibroin-doxorubicin, and silk fibroin-folate-doxorubicin nanoparticles after 7 and 14 days culture periods. Scale bar represents 100 μm.

coculture constructs are less as compared to respective controls (Figure 1). As observed, osteoblast constructs show maximum proliferation after every kind of treatment, in comparison to the cancerous and coculture constructs. Coculture constructs exhibits comparable cell growth with cancerous constructs for all three kinds of treatment, However, the SF-FA-DOX-NP treated samples exhibit lowest amount of cell growth and proliferation both after 7 and 14 day. The cell proliferation profile of 7th and 14th day construct is similar in context with nontreated constructs.

b. Cellular Distribution in Monoculture and Coculture Constructs. Prestained cells with cell tracker dye green (osteoblast) and red (breast cancer cells) are used to visualize the effect of drug treatment (pure doxorubicin, nontargeted doxorubicin and targeted doxorubicin) on cellular distribution and cell growth in monoculture and coculture constructs. Figure 2A reveals that the cell proliferation and the density of coculture construct are less as compared to osteoblast monoculture construct. The cell morphology and density of osteoblast like cells are not much affected with pure doxorubicin, non targeted doxorubicin and targeted doxorubicin, while the breast cancer cell distribution is affected drastically.

c. Scanning Electron Microscopy. The effect of drug on cell morphology is evaluated by scanning electron microscopy. As observed in Figure 2B, it is clear that after treatment with pure drug, nontargeted, and targeted drug, the cells morphology altered visibly in monoculture (cancer) and coculture constructs but not in osteoblast monoculture. The drug treated cancer and coculture cells show distorted morphology and reduced cell number.

DOI: 10.1021/am506094c
ACS Appl. Mater. Interfaces 2015, 7, 2269−2279

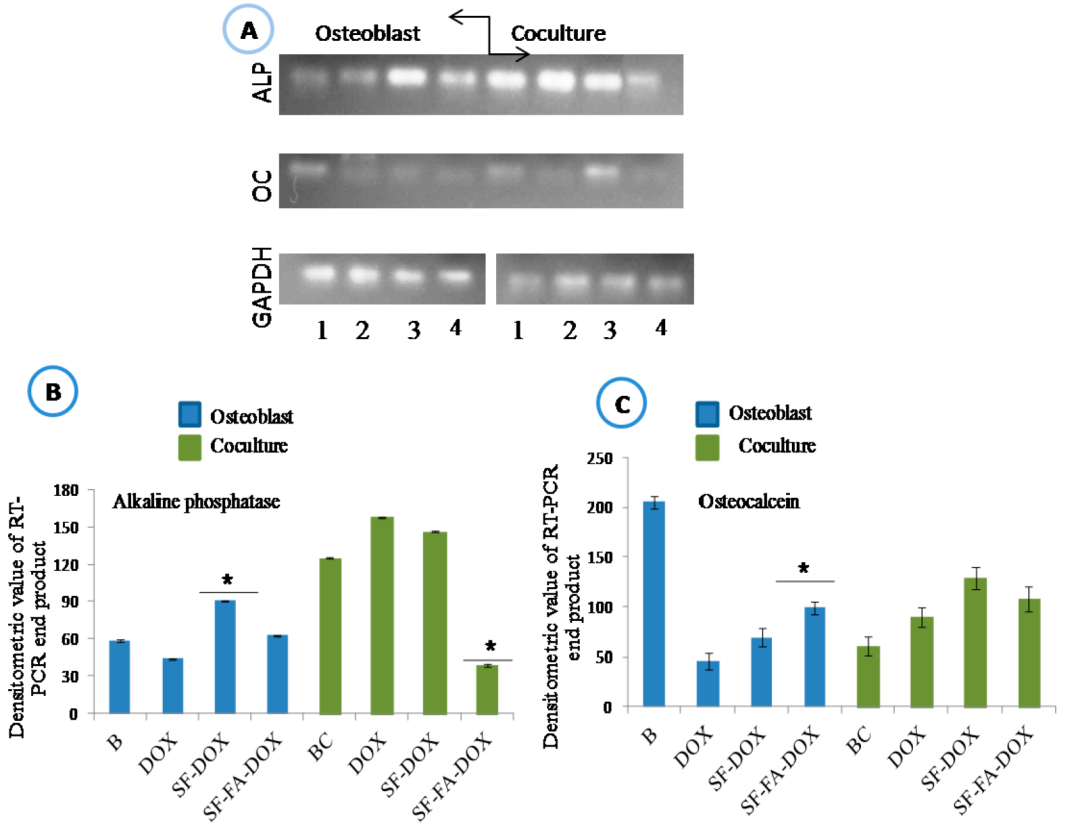

Figure 4. Transcription level analysis of osteogenesis related genes in bone cancer metastasis, osteoblast cells and coculture cell seeded construct. (A) Representative electrophoretic images from the reverse transcriptase polymerase chain reaction (RT-PCR) show for bone alkaline phosphatase, osteocalcein (OC) and GAPDH. The lanes are designated as control (1), treated with doxorubicin (2), silk fibroin-doxorubicin (3), silk fibroin-folate-doxorubicin (4). (B) GAPDH normalized densitometric quantification of PCR product for alkaline phosphatase and (C) osteoclacein gene expression, by using Image j software. Where "B" represent the bone cells and "BC" represents both the bone and cancer cells.

3.2. Osteogenesis in Drug Treated Scaffold. *a. Alkaline Phosphatase Synthesis.* Figure 3A reveals the level of secreted alkaline phosphatase (ALP) from coculture and monoculture constructs. The result indicates that the pure drug, nontargeted drug, and targeted drug do not affect the alkaline phosphatase secretion in osteoblast monoculture construct after 7 and 14 day time periods. However, the secretion of ALP in control (without drug) coculture construct is significantly higher than the osteoblast monoculture samples. ALP secretion is reduced in coculture constructs after the addition of the pure, non-targeted and targeted drugs. Among three kinds of treatment, the targeted drug delivery significantly ($p < 0.05$) lowers the ALP secretion.

b. Calcium Deposition Assay. Mineralization or deposition of calcium by the osteoblast like cells is compared with the treated and nontreated coculture constructs using Alizarin Red staining. Representative images of stained constructs (Figure 3B) are attributed to the formation of calcium nodules on the constructs. The drug treated constructs do not show any deleterious effect on bone mineralization after day 7 and 14. The mineralization is higher in day 14 culture period as shown by the dense coverage of calcium deposits (Figure 3B).

c. Analysis of Osteogenic Markers. To evaluate the expression of osteogenic markers in treated coculture and monoculture constructs (osteoblast like cells) semi quantative RT PCR is carried out. The level of ALP mRNA is increased in coculture constructs and reduced in targeted drug delivery sample (Figure 4A and 4B). The expression of osteocalcein (OC) in mono (osteoblast) and coculture construct does not alter significantly after drug treatment (Figure 4A,C).

3.3. Analysis of Invasive Properties of the Metastatic Breast Cancer Cells. *a. Angiogenesis.* To study the effect of drug on angiogenesis and metastasis factors on 3D fibroin matrices cultured with coculture and monoculture cancer constructs. The ELISA assay is carried out for the VEGF quantification. Figure 5A shows that the use of the pure drug, nontargeted drug, and targeted drug lowered the production of VEGF in both monoculture and coculture constructs. The VEGF production is significantly higher ($p < 0.05$) in non treated cancer cells and coculture cells after day 7 as compared to day 14 culture period.

b. Glucose Consumption and Lactate Production. To investigate the effect of drug treatment on glucose metabolism and lactate production in monoculture and coculture constructs, the glucose consumption and lactate production assay are carried out after 7 and 14 days. The amount of glucose consumed and lactate produced by cells on drug treated silk fibroin matrices is comparable to that of control. The glucose consumption and lactate production are significantly more in nontreated cells. The drug treated cells consume less glucose and produced low lactate after 7 and 14 day culture periods (Figure 5B,C).

4. DISCUSSIONS

Preclinical evaluation of the fabricated drug loaded nanoparticles is necessary to ensure patient's safety.[48] The Drug loaded folate conjugated nanoparticles show higher impact on the 2D system; however, they may exhibit contradictory effects in vivo. To bridge

DOI: 10.1021/am506094c
ACS Appl. Mater. Interfaces 2015, 7, 2269−2279

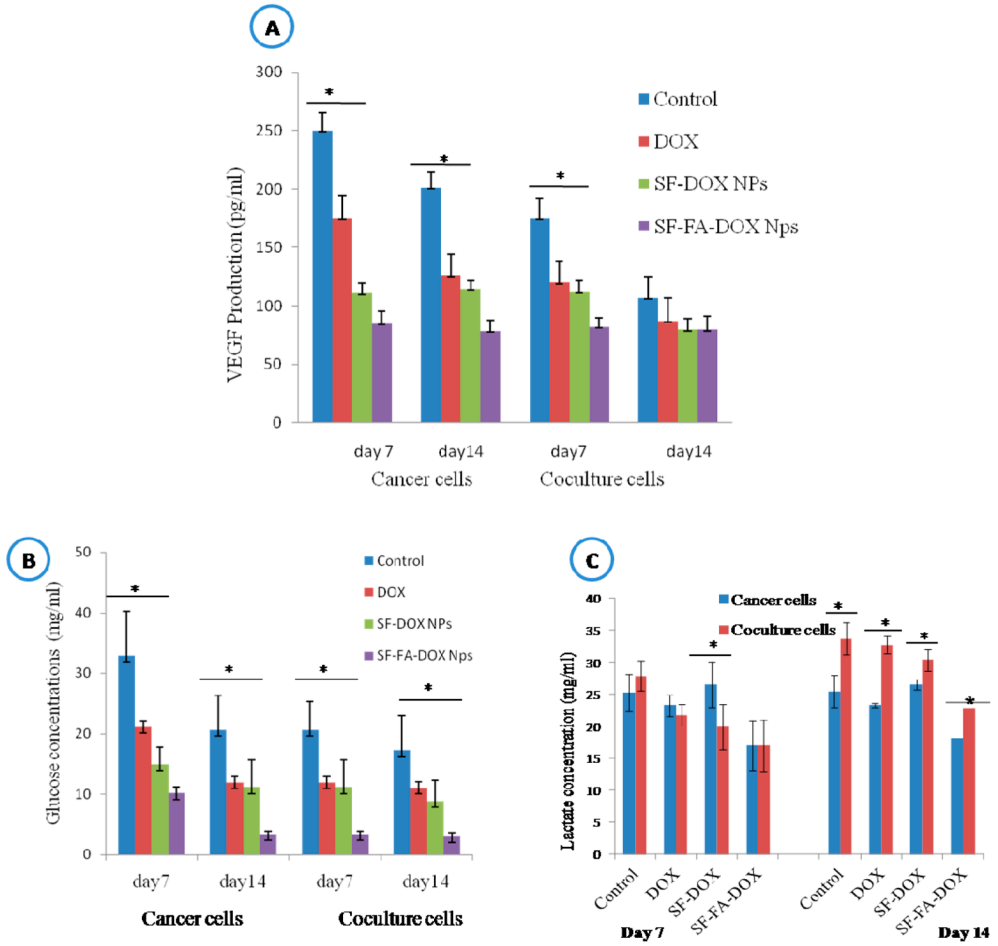

Figure 5. Functional assay of cancerous cells in co and mono culture construct. (A) Analysis of VEGF (angiogenic factor) secretion, (B) glucose metabolism, and (C) lactate production from monoculture (MDA-MB-231) and coculture (MDA-MB-231/MG63) construct after treatment (with pure doxorubicin (DOX), silk fibroin-doxorubicin (SF-DOX) and silk fibroin-folate doxorubicin (SF-FA-DOX) and untreated condition after day 7 and 14. Glucose and lactate concentration are quantified in mg/mL. The data is represented as mean ± SD (n = 3).

the gap between the conventional 2D system and the expensive animal model the 3D culture systems are utilized to evaluate the drug efficacy. The development of such an in vitro model may recapitulate the native tumor organization and other tissue microenvironment interaction as expected in vivo. Doxorubicin loaded folate conjugated silk fibroin nanoparticles successfully show their impact on the 2D system.[10] The present work deals with 3D silk scaffold as a viable and cost-effective tumor model in vitro before proceeding for animal model trial. This silk protein fibroin based 3D distribution model of cancer cells may reduce time, energy and expenditure. The cell seeded 3D in vitro tumor model show to represent the distinct tumorgenic zone (namely proliferative zone and necrotic) in context of cellular growth and distribution.[2] Silk based 3D in vitro bone-cancer cell distribution model are used to further evaluate the efficacy of the this drug delivery system.

In our previous report we fabricated the silk fibroin nanoparticles by desolvation method. The silk fibroin particles are activated using 2,2′-(ethylenedioxy)-bis(ethylamine) in the presence of ethylene dicarbodimide (EDC) and *N*-hydroxy scucinamide (NHS) as an intermediate. Further the folic acid is added in the presence of EDC/NHS (intermediate) to fabricate the folate conjugated silk fibroin nanoparticles.[10] The silk fibroin-folate conjugated nanoparticles are characterized in detail by TEM and dynamic light scattering (DLS). The conjugation of silk fibroin with folate is confirmed by FTIR spectroscopy. The pure silk fibroin (SF) and silk fibroin folate (SF-FA) conjugated nanoparticles are <200 nm in diameter. The particles are almost uniform and spherical in shape. The stability of the particles is confirmed by zeta potential. The surface potential of SF and SF-FA conjugated nanoparticles are −22 ± 5 and −32 ± 3 mV, respectively. The particle size and surface potential of the particles provide the stability to the particles and prevent any type of aggregation/agglomeration.

The 3D coculture models are becoming ideal for migration and proliferation analysis as well as to investigate the cellular interaction. The prestained osteoblast and breast cancer cells exhibit the distribution of cells within the pores of the scaffolds both in monoculture and coculture conditions. The cell metabolic assay (Figure 1A) indicates that the effect of drug on monoculture osteoblast like cells is comparatively less than coculture cells (Figure 1A). This may be due to presence of more folate receptors at the cancerous site, which helps in targeted delivery of the drug to the site of action and supports the hypothesis of using target specific delivery. The relative percent viability of cancerous cells in mono and coculture constructs is decreased after 14 days of culture as compared to day 7 of culture. The silk fibroin-folate doxorubicin (targeted) more effectively targets the cancerous cells in monoculture and coculture

DOI: 10.1021/am506094c
ACS Appl. Mater. Interfaces 2015, 7, 2269−2279

constructs compared to the nontargeted doxorubicin ($p < 0.05$). The IC_{50} (~6.03 ± 1.003 μg/mL) value of targeted doxorubicin in 3D culture system is 10-fold higher than the 2D system as observed earlier. Higher IC_{50} value for 3D culture system may be due to the 3D environment which mimics closely the in vivo tumor environment. Our observation are in line with earlier reports, where increased IC_{50} values are obtained in 3D in vitro tumor model.[43−48] In 3D system number of cells are higher and the poor penetration of the drug/np composite can also be an important reason for the decreased cytotoxicity. Higher concentrations of drugs are required to evaluate cytotoxicity.[48] The effect of folate conjugated anticancerous drug on 3D system is lowered as compared to 2D system reported earlier.[48,49] However, pure doxorubicin, nontargeted and targeted doxorubicin treated cancerous cells in both coculture and monoculture sample show distorted/constricted morphology (Figure 2A,B). The microscopic observation reveals that the cell attachment and morphology of monoculture osteoblast like cells are not much affected when they are treated with any kind of doxorubicin. The constructs also show avascular tumor like morphology, which also contributes to their aggressiveness and drug resistance. Higher doses of the drug are required to achieve comparable reduction in cell viability and invasive potential in 3D culture. The cell growth pattern in 3D scaffolds is probably more suitable for the long-term growth of the cancerous cells. The 3D cell aggregation leads to hypoxia in the tumor center and the interaction between the cell and ECM may also alter the drug response.[50] The results obtained are supported by others where tumor cells grown in 3D system develop multicellular resistance to most cytotoxic drugs compared to those grown in monolayer culture.[51]

The interaction of the breast cancer cells with osteoblast like cells and the secreted factors from the cancer cells may influence the osteoblast growth and bone resorption.[52] In the present study the anticancer drug treated monoculture and coculture constructs significantly affect the alkaline phosphatase secretion ($p < 0.05$). The untreated cocultured constructs show a substantial increase in alkaline phosphatase (ALP) secretion than osteoblast only constructs (Figure 3A). This result is supported by earlier observation where higher ALP secretion from coculture is attributed to the early phase of osteogenic differentiation.[51] The ALP quantification data are also supported by the semiquantitative RT-PCR, where ALP mRNAs are up regulated in coculture construct (Figure 4A,B; Table 2). ALP is essential for the initiation of bone mineralization in early stages of osteogenesis and found to be elevated in bone cancer patients. The mRNA level of osteocalcein is not changed in coculture and the drug treated condition (Figure 4A,C). The up-regulations of ALP in coculture condition may be due to the bone metastasis even after the drug treatment. The results are similar to the earlier reports where the expression of ALP is higher than osteocalcein.[53] The targeted nanoparticles with drug do not exhibit any significant effect on the osteoblast specific genes. We cannot rule out the deleterious effects of this drug, which may demonstrate itself in the long term investigation. The drug treated constructs exhibit similar level of bone mineralization as observed in control samples. No significance difference is observed in terms of bone mineralization between the treated and untreated monoculture and coculture cells. This indicates that the drug treated constructs has no significant effect on bone mineralization (Figure 3B).

Table 2. Primers Used for Semiquantative RT-PCR

gene name	gene sequences (5′-3′)	size	primer size
alkaline phosphatase	forward primer tgcgcagagaaagagaaagacccca	156 bp	25, 21 bp
	reverse primer ggcagccgtcactgtggagac		
osteocalcein	forward primer cagccgcagctcccaaccac	173 bp	20, 21 bp
	reverse primer cgccagcctccagcactgttt		
GAPDH	forward primer aattgagcccgcagcctccc	153 bp	20, 20 bp
	reverse primer ccaggcgcccaatacgacca		

To analyze the tumor metastatic markers such as angiogenesis and high metabolism the vascular endothelial growth factor (VEGF) secretion and glucose metabolism are investigated in both monoculture (cancer cell) and coculture constructs. The VEGF overexpression in tumors is associated with the increased angiogenesis, proliferation and metastasis.[53] The release of vascular endothelial growth factor from untreated monoculture cancerous cells and coculture cells are higher in both 7th and 14th day of culture. Pure doxorubicin, nontargeted and targeted doxorubicin show less angiogenesis in monoculture and coculture treated cells in context of the VEGF secretion (Figure 5A). Less production of the VEGF from the drug treated cells may be due to down regulation of pro-angiogenic factors.[54] The targeted nanoparticles with drug are able to effectively target the cancer cells in monoculture and coculture constructs.

Rapidly proliferating cancerous cells consume high level of glucose and produce a higher amount of lactate after 7th and 14th days of culture. The glucose consumption and lactate production are less in drug treated monoculture cancerous cells and coculture cells. A smaller amount of glucose is consumed and lactate produced by the cells treated with drug loaded targeted nanoparticles (Figure 5B,C). This may be due to the induction of oxidative damage by chemotherapeutic drugs, which create an antitumor effect.[55,56] Our results indicate that the invasive properties of the metastatic breast cancer cells are significantly affected after the delivery of the drug from the fibroin-folate conjugated nanoparticles.

5. CONCLUSIONS

A 3D silk fibroin scaffold based coculture model is designed to observe the interactions of the cancerous cells within the bone microenvironment. The effects of targeted delivery of doxorubicin loaded folate conjugated fibroin nanoparticles on the cancerous cell growth in coculture construct are observed. The coculture of cancer cells with the osteoblast-like cells exhibit the decreased population of the cancerous cells, invasiveness and angiogenesis (in terms of VEGF secretion) after the treatment. The proliferation and function of bone cells remains mostly unaffected after the treatment, however, cohabitation with the cancer cells seems to affect the bone cell mRNA level and alkaline phosphatase secretion. The experimental observations indicate that the drug loaded folate conjugated nanoparticles effectively target the cancer cells in bone metastasis 3D in vitro systems. This 3D distribution system may be utilized as a 3D matrix for the coculture model in cancer research. This natural silk based 3D distribution system of cell culture can easily be exploited as a high throughput screening system for cancer drug discovery and development.

AUTHOR INFORMATION

Corresponding Author

*E-mail: kundu@hijli.iitkgp.ernet.in. Tel: +91-3222-283764.

DOI: 10.1021/am506094c
ACS Appl. Mater. Interfaces 2015, 7, 2269−2279

Funding

This work is financially supported by the Indian Council of Medical Research and Department of Biotechnology, Govt. of India.

Notes

The authors declare no competing financial interest.

■ ACKNOWLEDGMENTS

This work is financially supported by the Indian Council of Medical Research and Department of Biotechnology, Govt. of India.

■ REFERENCES

(1) She, W.; Li, N.; Luo, K.; Guo, C.; Wang, G.; Geng, Y.; Gu, Z. Dendronized Heparin Doxorubicin Conjugate Based Nanoparticle as pH-Responsive Drug Delivery System for Cancer Therapy. *Biomaterials* **2013**, *34*, 2252−2264.

(2) Huang, C. W.; Lin, F. M.; Chang, T. H.; Liao, K. W.; Huang, H. D. Identifying Cancer Highly-Expressed Membrane Receptors for Targeted Drug Delivery. *Int. J. Bioinform. Res. Appl.* **2012**, *8*, 192−209.

(3) Subia, B.; Kundu, S. C. Drug Loading and Release on Tumor Cells using Silk fibroin−Albumin Nanoparticles as Carriers. *Nanotechnology* **2013**, *24*, 035103.

(4) Zwicke, G. L.; Mansoori, G. Ali.; Jeffery, C. J. Utilizing the Folate Receptors for Active Targeting of Cancer Nanotherpautics. *Nano Rev.* **2012**, *3*, PMC3521101.

(5) Yang, S. J.; Lin, F. H.; Tsai, K. C.; Wei, M. F.; Tsai, H. M.; Wong, J. M.; Shieh, M. Folic Acid-Conjugated Chitosan Nanoparticles Enhanced Protoporphyrin IX Accumulation in Colorectal Cancer Cells. *J. Bioconjugate Chem.* **2010**, *21*, 667−689.

(6) Zhang, Y.; Hong, H.; Myklejord, D. V.; Cai, W. Molecular Imaging with SERS-Active Nanoparticles. *Small* **2011**, *7*, 3261−3269.

(7) Provenzale, J. M.; Silva, G. A. Use of Nanoparticles for Central Nervous System Imaging and Therapy. *A. J. Nanotechnol.* **2009**, *30*, 1293−1301.

(8) Song, H.; Su, C.; Cui, W.; Zhu, B.; Liu, L.; Chen, Z.; Zhao, L. Folic acid-Chitosan Conjugated Nanoparticles for Improving Tumor-Targeted Drug Delivery. *BioMed. Res. Int.* **2013**, *723*, 158−1564.

(9) Du, C.; Deng, D.; Shan, L.; Wan, S.; Cao, J.; Tian, J.; Gu, Y. A pH-Sensitive Doxorubicin Prodrug Based on Folate-Conjugated BSA for Tumor-Targeted Drug Delivery. *Biomaterials* **2013**, *34*, 3087−3097.

(10) Subia, B.; Chandra, S.; Talukdar, S.; Kundu, S. C. Folate Conjugated Silk Fibroin Nanocarriers for Targeted Drug Delivery. *Integr. Biol.* **2014**, *6*, 203−214.

(11) Gao, W.; Xiang, B.; Meng, T. T.; Liu, F.; Qi, X. R. Chemotherapeutic Drug Delivery to Cancer Cells Using a Combination of Folate Targeting and Tumor Microenvironment-Sensitive Polypeptides. *Biomaterials* **2013**, *34*, 4137−4149.

(12) Shinoda, T.; Takagi, A.; Maeda, A.; Kagatani, S.; Konno, Y.; Hashida, M. *In Vivo* Fate of Folate-BSA in Non-Tumor and Tumor Bearing Mice. *J. Pharm. Sci.* **1998**, *87*, 1521−1526.

(13) Yoo, H. S.; Park, T. G. Folate Receptor Targeted Biodegradable Polymeric Doxorubicin Micelles. *J. Controlled Release* **2004**, *96*, 273−283.

(14) Lee, E. S.; Na, K.; Bae, Y. H. Doxorubicin Loaded pH-Sensitive Polymeric Micelles for Reversal of Resistant MCF-7 Tumor. *J. Controlled Release* **2005**, *103*, 405−418.

(15) Paulos, C. M.; Reddy, J. A.; Leamon, C. P.; Turk, M. J.; Low, P. S. Ligand Binding and Kinetics of Folate Receptor Recycling *In Vivo*: Impact on Receptor-Mediated Drug Delivery. *Mol. Pharmacol.* **2004**, *66*, 1406−1414.

(16) Xu, S.; Olenyuk, B. Z.; Okamoto, C. T.; Hamm-Alvarez, S. F. Targeting Receptor Mediated Endocytosis Pathways with Nanoparticles: Rationale and Advances. *Adv. Drug Delivery Rev.* **2013**, *65*, 121−138.

(17) Szot, C. S.; Buchanan, C. F.; Freeman, J. W.; Rylander, M. N. 3D *In Vitro* Bioengineered Tumors Based on Collagen I Hydrogels. *Biomaterials* **2011**, *32*, 7905−7912.

(18) Birgersdotter, A.; Sandberg, R.; Ernberg, I. Gene Expression Perturbation *In Vitro*-A Growing Case for Three Dimensional (3D) Culture Systems. *Semin. Cancer Biol.* **2005**, *15*, 405−412.

(19) Weigelt, B.; Bissell, M. J. Unraveling The Micro-Environmental Influences on The Normal Mammary Gland and Breast Cancer. *Semin. Cancer Biol.* **2008**, *18*, 311−321.

(20) Kim, J. B. Three-Dimensional Tissue Culture Models in Cancer Biology. *Semin. Cancer Biol.* **2005**, *15*, 365−377.

(21) Sieh, S.; Taubenberger, A. V.; Lehman, M. L.; Clements, J. A.; Nelson, C. C.; Hutmacher, D. W. Paracrine Interactions Between LnCAP Prostate Cancer Cells and Bioengineered Bone in 3D *In Vitro* Culture Reflect Molecular Changes During Bone Metastasis. *Bone* **2014**, *S8*, 756−782.

(22) Nyga, A.; Cheema, U.; Loizidou, M. 3D Tumour Models: Novel *In Vitro* Approaches to Cancer Studies. *J. Cell Commun. Signal.* **2013**, *5*, 239−248.

(23) Marlow, R.; Honeth, G.; Lombardi, S.; Cariati, M.; Hessey, S. M.; Pipili, A.; Mariotti, V.; Buchupalli, B.; Foster, K.; Bonnet, D.; Grigoriadis, A.; Purushotham, A.; Tutt, A.; Dontu, G. A Novel Model of Dormancy for Bone Metastatic Breast Cancer Cells. *Cancer Res.* **2013**, *73*, 6886−6899.

(24) Zhang, M.; Boughton, P.; Rose, B.; Lee, S.; Hong, M. A. The Use of Porous Scaffold as a Tumor Model. *Int. J. Biomater.* **2013**, 396056−396065.

(25) Talukdar, S.; Kundu, S. C. Engineered 3D Silk-Based Metastasis Models: Interactions Between Human Breast Adenocarcinoma, Mesenchymal Stem Cells and Osteoblast-Like Cells. *Adv. Funct. Mater.* **2013**, *23*, 5249−5260.

(26) Mandal, B. B.; Kundu, S. C. Non-Bioengineered Silk Gland Fibroin Protein: Characterization and Evaluation of Matrices for Potential Tissue Engineering Applications. *Biotechnol. Bioeng.* **2008**, *100*, 1237−1250.

(27) Talukdar, S.; Mandal, M.; Hutmacher, D. W.; Russell, P. J.; Soekmadji, C.; Kundu, S. C. Engineered Silk Fibroin Protein 3D Matrices for *In Vitro* Tumor Model. *Biomaterials* **2011**, *32*, 2149−2159.

(28) Baker, E. L.; Lu, J.; Yu, D.; Bonnecaze, R. T.; Zaman, M. H. Cancer Cell Migration: Integrated roles of Matrix Mechanism and Transformation Potential. *Biophys. J.* **2010**, *99*, e20355.

(29) McKnight, A. L.; Kugel, J. L.; Rossman, P. J.; Manduca, A.; Hartmann, L. C.; Ehman, R. L. MRI Elastography of Breast Cancer Preliminary Results. *Am. J. Roentgenol.* **2002**, *178*, 1411−1417.

(30) Talukdar, S.; Kundu, S. C. Non Mulberry Silk Fibroin Protein Based *In Vitro* Tumor Model for Evaluation of Anticancer Drug Delivery. *Adv. Funct. Mater.* **2012**, *22*, 4778−4788.

(31) Mandal, B. B.; Kundu, S. C. Non Mulberry Silk Gland Fibroin Protein 3D Scaffolds for Enhanced Differentiation of Human Mesenchymal Stem Cells into Osteocytes. *Acta Biomater.* **2009**, *5*, 2579−2590.

(32) Kleinman, H. K.; Martin, G. R. Matrigel: Basement Membrane Matrix with Biological Activity. *Semin. Cancer Biol.* **2005**, *15*, 378−386.

(33) Zhao, Y.; Yao, R.; Ouyang, L.; Ding, H.; Zhang, T.; Zhang, K.; Cheng, S.; Sun, W. Three-Dimensional Printing of HeLa Cells for Cervical Tumor Model *In Vitro*. *Biofabrication* **2014**, *6*, 035001.

(34) Fischbach, C.; Chen, R.; Matsumoto, T.; Schmelzle, T.; Brugge, J. S.; Polverini, P. J.; Mooney, D. J. Engineering Tumors with 3D Scaffolds. *Nat. Methods* **2007**, *4*, 855−860.

(35) Ma, L.; Barker, J.; Zhou, C.; Li, W.; Zhang, J.; Lin, B.; Foltz, G.; Küblbeck, J.; Honkakoski, P. Towards Personalized Medicine with A Three-Dimensional Micro-Scale Perfusion-Based Two-Chamber Tissue Model System. *Biomaterials* **2012**, *33*, 4353−4361.

(36) Sieh, S.; Taubenberger, A. V.; Lehman, M. L.; Clements, J. A.; Nelson, C. C.; Hutmacher, D. W. Paracrine Interactions Between LnCAP Prostate Cancer Cells and Bioengineered Bone in 3D *In Vitro* Culture Reflect Molecular Changes During Bone Metastasis. *Bone* **2014**, *63*, 121−131.

DOI: 10.1021/am506094c
ACS Appl. Mater. Interfaces 2015, 7, 2269−2279

(37) Lescarbeau, R. M.; Seib, F. P.; Prewitz, M.; Werner, C.; Kaplan, D.L. *In Vitro* Model of Metastasis to Bone Marrow Mediates Prostate Cancer Castration Resistant Growth through Paracrine and Extracellular Matrix Factors. *PLoS One* **2012**, *7*, e40372.
(38) Horning, J. L.; Sahoo, S. K.; Vijayaraghavalu, S.; Dimitrijevic, S.; Vasir, J. K.; Jain, T. K.; Panda, A. K.; Labhasetwar, L. 3D Tumor Model for *In Vitro* Evaluation of Anticancer Drugs. *Mol. Pharmaceutics* **2008**, *5*, 849−862.
(39) Talukdar, S.; Kundu, S. C. Engineered 3D Silk-Based Metastasis Models: Interactions Between Human Breast Adenocarcinoma, Mesenchymal Stem Cells and Osteoblast-Like Cells. *Adv. Funct. Mater.* **2013**, *23*, 5249−5260.
(40) Dhiman, H. K.; Ray, A. R.; Panda, A. K. Three-Dimensional Chitosan Scaffold-Based MCF-7 Cell Culture for the Determination of the Cytotoxicity of Tamoxifen. *Biomaterials* **2005**, *26*, 979−986.
(41) Dunne, L. W.; Huang, Z.; Meng, W.; Fan, X.; Zhang, N.; Zhang, Q.; An, Z. Human Decellularised Adipose Tissue Scaffold as a Model for Breast Cancer Cell Growth and Drug Treatments. *Biomaterials* **2014**, *35*, 4940−4990.
(42) Shin, C. S.; Kwak, B.; Han, B.; Park, K. Development of an *In Vitro* 3D Tumor Model to Study Therapeutic Efficiency of an Anticancer Drug. *Mol. Pharmaceutics* **2013**, *10*, 102−140.
(43) Talukdar, S.; Kundu, S. C. A Non-Mulberry Silk Fibroin Protein Based 3D *In Vitro* Tumor Model for Evaluation of Anticancer Drug Activity. *Adv. Funct. Mater.* **2012**, *22*, 4778−4788.
(44) Gupta, V.; Mun, G. H.; Choi, B.; Aseh, A.; Mildred, L.; Patel, A.; Zhang, Q.; Price, J. E.; Chang, D.; Robb, G.; Mathur, A. B. Repair and Reconstruction of a Resected Tumor Defectusing a Composite of Tissue Flap−Nanotherapeutic−Silk Fibroin and Chitosan Scaffold. *Ann. Biomed. Eng.* **2011**, *39*, 2374−2387.
(45) El-Dakdouki, M. H.; Xia, J.; Zhu, D. C.; Kavunja, H.; Grieshaber, J.; O'Reilly, S.; McCormick, J. J.; Huang, X. Assessing the *In Vivo* Efficacy of Doxorubicin Loaded Hyaluronan Nanoparticles. *ACS Appl. Mater. Interfaces* **2014**, *6* (1), 697−705.
(46) Chen, M.; Le, D.; Hein, S.; Li, P.; Nygaard, J. V.; Kassem, M.; Kjems, J.; Besenbacher, F.; Bünger, C. Fabrication and Characterization of a Rapid Prototyped Tissue Engineering Scaffold with Embedded Multicomponent Matrix for Controlled Drug Release. *Int. J. Nanomed.* **2012**, *7*, 4285−4297.
(47) Ricketts, K. P. M.; Cheema, U.; Nyga, A.; Castoldi, A.; Guazzoni, C.; Magdeldin, T.; Emberton, M.; Gibson, A. P.; Royle, G. J.; Loizidou, M. A 3D *In Vitro* Cancer Model as a Platform for Nanoparticle Uptake and Imaging Investigations. *Small* **2014**, DOI: 10.1002/smll.201400194.
(48) Godugu, C.; Patel, A. R.; Desai, U.; Andey, T.; Sams, A.; Singh, M. Algi-Matrix Based 3D Cell Culture System as an *In-Vitro* Tumor Model for Anticancer Studies. *PLoS One* **2013**, *8* (1), e53708.
(49) Sarkar, B.; Dosch, J.; Simeone, D. M. Cancer Stem Cells: A New Theory Regarding a Timeless Disease. *Chem. Rev.* **2009**, *109*, 3200−3208.
(50) Johnson, A. W.; Hraley, B. Cell Death Signaling and Anticancer Therapy. *Anticancer Res.* **2011**, *31*, 3237−3247.
(51) Weigelt, B.; Bissell, M. J. Unraveling the Micro-Environmental Influences on The Normal Mammary Gland and Breast Cancer. *Semin Cancer Biol.* **2008**, *18*, 311−321.
(52) Wang, N.; Wang, X.; Xing, C.; Sun, B.; Yu, X.; Hu, J.; Liu, J.; Zeng, M.; Xiong, M.; Zhou, S.; Yang, J. Role of TGF-beta1 in Bone Matrix Production in Vascular Smooth Muscle Cells Induced by a High-Phosphate environment. *Nephron* **2010**, *115*, e60−68.
(53) Magnusson, P.; Larsson, L.; Englund, G.; Larsson, B.; Lena, S. S.; Peter, S. Differences of Bone Alkaline Phosphatase Isoforms in Metastatic Bone Disease and Discrepant Effects of Clodronate on Different Skeletal Sites Indicated by the Location of Pain. *Clin. Chem.* **1998**, *44*, 1621−1628.
(54) Fantozzi, A.; Gruber, D. C.; Pisarsky, L.; Heck, C.; Kunita, A.; Yilmaz, M.; Meyer-Schaller, N.; Cornille, K.; Hopfer, U.; Bentires-Alj, M.; Christofori, G. VEGF-Mediated Angiogenesis Links Emt-Induced Cancer Stamens to Tumor Initiation. *Cancer Res.* **2014**, *1*, 1566−1575.
(55) Ma, J.; Waxman, D. J. Combination of Anti-Angiogenesis with Chemotherapy for More Effective Cancer Treatment. *Mol. Cancer* **2008**, *7*, 3670−3684.
(56) Zhao, Y.; Butler, E. B.; Tan, M. Targeting Cellular Metabolism to Improve Cancer Therapeutics. *Cell Death Dis.* **2013**, *4*, e532.

DOI: 10.1021/am506094c
ACS Appl. Mater. Interfaces 2015, 7, 2269−2279